Full-Wave Verification of an Electromagnetic Inversion Metasurface Design Method

Trevor Brown, Ziqi Liu, and Puyan Mojabi
Department of Electrical and Computer Engineering, University of Manitoba, Winnipeg, MB, Canada

***Abstract*—This paper summarizes, extends, and synthetically evaluates a method for metasurface design which uses electromagnetic inversion. After the inversion algorithm determines a homogenized surface susceptibility model to implement a desired power pattern, the susceptibility distribution is converted to a three-layer admittance sheet topology. Lastly, full-wave commercial software is used to simulate and verify the performance of a metasurface designed and implemented using the proposed procedure.**

I. Introduction

Metasurfaces can facilitate the systematic control of electromagnetic fields with numerous applications reported in the past decade [1]–[5]. Recently, the electromagnetic inversion framework has been proposed as a design tool to determine a homogenized metasurface model [6], [7]. The main advantage of this framework lies in its ability to work with a variety of desired specifications given on arbitrary specification domains. For example, the specifications could be desired power patterns (no phase information), or more practically performance criteria such as half-power-beamwidth and null locations. Note that these types of specifications do not directly translate into the required tangential fields on the surface of the metasurface, thus, justifying the use of the inversion framework.

An overview of the steps involved in the inversion approach is shown in Figure 1. First, we minimize a cost functional that quantifies the difference between the desired data and simulated data due to a set of equivalent electric and magnetic currents $\vec{J}$ and $\vec{M}$ [7]. The currents found from this stage are used as the initial guess for the second optimization stage that takes the incident field into consideration and uses particle swarm optimization (PSO) to enforce local power conservation (LPC), a necessary condition for a passive and lossless metasurface [8]. The currents found in the second stage are then used to compute the transmitted fields on the output side of the metasurface, assuming Love's equivalence condition was enforced [7]. The final stage consists of computing the surface susceptibilities ($\overline{\overline{\chi}}_{\text{ee}}, \overline{\overline{\chi}}_{\text{em}}, \overline{\overline{\chi}}_{\text{mm}}, \overline{\overline{\chi}}_{\text{me}}$) from the generalized sheet transition conditions (GSTCs). As reported in [8], to ensure a lossless and passive metasurface we impose that $\overline{\overline{\chi}}_{\text{ee}}$ and $\overline{\overline{\chi}}_{\text{mm}}$ are completely real. Since the field transformation satisfies LPC, $\overline{\overline{\chi}}_{\text{em}}$ and $\overline{\overline{\chi}}_{\text{me}}$ will necessarily be lossless. Furthermore, stipulating that $\overline{\overline{\chi}}_{\text{em}}$ and $\overline{\overline{\chi}}_{\text{me}}$ are purely imaginary ensures that the conditions for reciprocity are met as well. In this work, the surface susceptibility distributions found for a desired power pattern are verified by their implementation using a three-layer admittance sheet topology [9] in ANSYS HFSS.

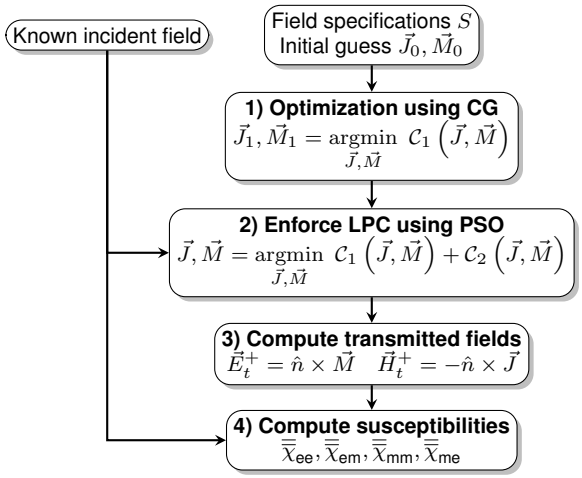

Fig. 1. Overview of the main steps involved in the electromagnetic inversion metasurface design procedure.

II. Conversion to Three-Layer Admittance Model

Assuming a 1D metasurface along $x = 0$ and 2D TE$_z$ fields for simplicity, the GSTCs can be reduced to

$$-\Delta H_z = (j\omega\epsilon_0 E_{y,\text{av}})\,\chi_{\text{ee}}^{yy} + (j\omega\sqrt{\mu_0\epsilon_0}H_{z,\text{av}})\,\chi_{\text{em}}^{yz} \quad (1a)$$

$$-\Delta E_y = (j\omega\mu_0 H_{z,\text{av}})\,\chi_{\text{mm}}^{zz} + (j\omega\sqrt{\mu_0\epsilon_0}E_{y,\text{av}})\,\chi_{\text{me}}^{zy}, \quad (1b)$$

where the Δ operator and 'av' subscript refer to the difference and average tangential fields across the metasurface, respectively. The expressions in (1) can be rearranged to produce the equivalent $ABCD$-parameter representation, which, assuming a reciprocal metasurface, results in

$$A = G^{-1}\left[\frac{k_0^2}{4}\chi_{\text{ee}}^{yy}\chi_{\text{mm}}^{zz} - \left(1 - \frac{jk_0}{2}\chi_{\text{em}}^{yz}\right)^2\right] \quad (2a)$$

$$B = G^{-1}\left[-j\omega\mu_0\chi_{\text{mm}}^{zz}\right] \quad (2b)$$

$$C = G^{-1}\left[-j\omega\epsilon_0\chi_{\text{ee}}^{yy}\right] \quad (2c)$$

$$D = G^{-1}\left[\frac{k_0^2}{4}\chi_{\text{ee}}^{yy}\chi_{\text{mm}}^{zz} - \left(1 + \frac{jk_0}{2}\chi_{\text{em}}^{yz}\right)^2\right], \quad (2d)$$

where k_0 is the wavenumber of free space and G is

$$G = -\left(\frac{k_0}{2}\chi_{\text{em}}^{yz}\right)^2 - \frac{k_0^2}{4}\chi_{\text{ee}}^{yy}\chi_{\text{mm}}^{zz} - 1. \quad (3)$$

Equating (2) with the $ABCD$-parameters of the cascaded admittance sheets [9] and analytically solving for the admittances

of the three layers denoted by Y_1, Y_2, and Y_3 results in

$$Y_1 = \frac{D - jZ_0 \sin(\beta l)\cos(\beta l)\, Y_2 - \cos^2(\beta l) + \sin^2(\beta l)}{2jZ_0 \sin(\beta l)\cos(\beta l) - Z_0^2 \sin^2(\beta l)\, Y_2} \tag{4a}$$

$$Y_2 = \frac{B - 2jZ_0 \sin(\beta l)\cos(\beta l)}{-Z_0^2 \sin^2(\beta l)} \tag{4b}$$

$$Y_3 = \frac{A - jZ_0 \sin(\beta l)\cos(\beta l)\, Y_2 - \cos^2(\beta l) + \sin^2(\beta l)}{2jZ_0 \sin(\beta l)\cos(\beta l) - Z_0^2 \sin^2(\beta l)\, Y_2}, \tag{4c}$$

where β, l, and Z_0 are the propagation constant, thickness, and characteristic impedance of the substrate, respectively. It should be noted while this is not a manufacturable implementation, the admittance sheets could be physically implemented using metallic 'dogbone' traces or other structures [10], [11].

III. Full-Wave Simulated Example

The example presented here uses ANSYS HFSS to simulate a metasurface designed using the presented procedure and implementation. The metasurface is designed to transform an incident TE_z plane wave into the far-field (FF) power pattern (amplitude-only) shown in red in Figure 2 at a frequency of 10.5 GHz. The substrate used in simulation for the unit cells is Rogers RO3003 with $\epsilon_r = 3.0$ and $\tan\delta$ = 0.001, with each layer having a thickness of 60 mil. The metasurface, shown in Figure 3, is 5λ in length along the $x = 0$ line, and is composed of 30 unit cells each of width $\lambda/6$. Absorbing elements have been placed on either side of the metasurface and metallic baffles are placed between the unit cells as in [11]. First, the susceptibilities are found following the steps in Figure 1. Secondly, the three admittance values for each unit cell are found by evaluating (4) and implemented in HFSS using impedance boundary conditions. Figure 3 shows the result of illuminating the metasurface with a uniform plane wave. The corresponding FF pattern generated from the simulation is shown in Figure 2, along with the FF pattern generated by the equivalent currents after the PSO stage. The FF pattern from the equivalent currents demonstrates the concessions that must be made when enforcing local power conservation. Nonetheless, the FF from HFSS exhibits excellent agreement with the specified pattern within the main beam and minimal reflections are present.

IV. Conclusion

We presented an overview of a macroscopic design method that uses electromagnetic inversion to find a passive, lossless, and reciprocal metasurface model that satisfies some user-defined field specifications. Furthermore, the expressions necessary to implement each unit cell using a three-layer admittance sheet topology were presented and utilized. A full-wave simulated example was presented to verify the design method and implementation, exhibiting good agreement with the target field specifications. Future work will include physically implementing the three-layer admittance sheets using a three-layer dogbone structure [10], [11] and comparing experimental results with those obtained from simulation.

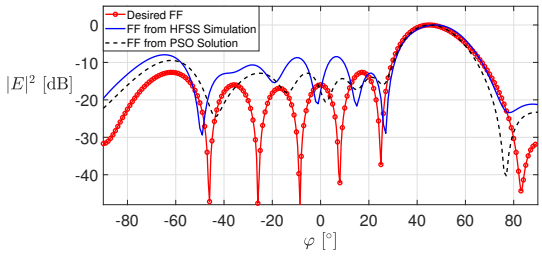

Fig. 2. Comparison of the far-field power pattern produced by the equivalent currents from the PSO stage (dashed black curve), the power pattern generated from the HFSS simulation of the resulting metasurface design (solid blue line), and the specified (target) power pattern (red line with circular markers).

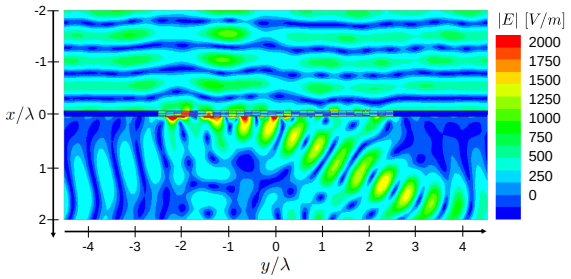

Fig. 3. HFSS simulation of the designed metasurface using the three-layer admittance sheet topology illuminated by a normally incident plane wave.

References

[1] C. L. Holloway, E. F. Kuester, J. A. Gordon, J. O'Hara, J. Booth, and D. R. Smith, "An overview of the theory and applications of metasurfaces: The two-dimensional equivalents of metamaterials," *IEEE Antennas and Propagation Magazine*, vol. 54, no. 2, pp. 10–35, 2012.

[2] C. Pfeiffer and A. Grbic, "Metamaterial Huygens' surfaces: Tailoring wave fronts with reflectionless sheets," *Phys. Rev. Lett.*, vol. 110, p. 197401, May 2013.

[3] M. Selvanayagam and G. Eleftheriades, "Discontinuous electromagnetic fields using orthogonal electric and magnetic currents for wavefront manipulation," *Optics Express*, pp. 14 409–14 429, 2013.

[4] S. Tretyakov, "Metasurfaces for general transformations of electromagnetic fields," *Philos. Trans. Royal Soc. A: Mathematical, Physical and Engineering Sciences*, vol. 373, no. 2049, p. 20140362, 2015.

[5] K. Achouri and C. Caloz, "Design, concepts and applications of electromagnetic metasurfaces," *Nanophotonics*, vol. 7, no. 6, pp. 1095–1116, 2018.

[6] T. Brown, C. Narendra, and P. Mojabi, "On the use of the source reconstruction method for metasurface design," *12th European Conference on Antennas and Propagation (EuCAP)*, pp. 302–306, April 2018.

[7] T. Brown, C. Narendra, Y. Vahabzadeh, C. Caloz, and P. Mojabi, "On the use of electromagnetic inversion for metasurface design," *IEEE Transactions on Antennas and Propagation*, pp. 1–13, 2019.

[8] T. Brown, Y. Vahabzadeh, C. Caloz, and P. Mojabi, "Enforcing local power conservation for metasurface design using electromagnetic inversion," *14th European Conference on Antennas and Propagation (EuCAP 2020)*, pp. 1–4, in press, 2020.

[9] J. P. Wong, A. Epstein, and G. V. Eleftheriades, "Reflectionless wide-angle refracting metasurfaces," *IEEE Antennas and Wireless Propagation Letters*, vol. 15, pp. 1293–1296, 2015.

[10] G. Lavigne, K. Achouri, V. S. Asadchy, S. A. Tretyakov, and C. Caloz, "Susceptibility derivation and experimental demonstration of refracting metasurfaces without spurious diffraction," *IEEE Transactions on Antennas and Propagation*, vol. 66, no. 3, pp. 1321–1330, 2018.

[11] G. Xu, S. V. Hum, and G. V. Eleftheriades, "Augmented Huygens' metasurfaces employing baffles for precise control of wave transformations," *IEEE Transactions on Antennas and Propagation*, vol. 67, no. 11, pp. 6935–6946, 2019.